Journal of Power Sources 193 (2009) 189–193

Contents lists available at ScienceDirect

Journal of Power Sources

journal homepage: www.elsevier.com/locate/jpowsour

Short communication

Structural and conductivity study of the proton conductor $BaCe_{(0.9-x)}Zr_xY_{0.1}O_{(3-\delta)}$ at intermediate temperatures

S. Ricote [a,b,*], N. Bonanos [b], M.C. Marco de Lucas [a], G. Caboche [a]

[a] Institut Carnot de Bourgogne, UMR 5209 CNRS-Université de Bourgogne, 9 Av. A. Savary, BP 47 870, F-21078 DIJON Cedex, France
[b] Fuel Cells and Solid State Chemistry Division, Risø National Laboratory for Sustainable Energy, Technical University of Denmark, P.O. 49, DK-4000 Roskilde, Denmark

ARTICLE INFO

Article history:
Received 2 October 2008
Received in revised form
10 November 2008
Accepted 11 November 2008
Available online 28 November 2008

Keywords:
High temperature proton conductor
Barium cerate
Barium zirconate
Phase transitions
Ionic conductivity
Electronic conductivity

ABSTRACT

The perovskite $BaCe_{(0.9-x)}Zr_xY_{0.1}O_{(3-\delta)}$ is prepared by solid-state reaction at 1400 °C and sintering at 1700 °C. It is characterised using X-ray diffraction, Raman spectroscopy and electrical measurements. A distortion from the cubic structure at room temperature is noticeable in the Raman spectra for $0.2 < x < 0.8$, but not in the X-ray diffraction patterns. This work points out the rhombohedral nature of this distortion. Phase transitions are studied up to 600 °C. The direct current conductivity is measured as a function of oxygen partial pressure, and at a water vapour partial pressure of 0.015 atm. The total conductivity is resolved into an ionic and a p-type component using a fitting procedure appropriate to the assumed defect model. The first contribution is useful for estimating the proton transport number, while the value of the second one should not be too high not to deteriorate the electrodes performance.

1. Introduction

Fuel cells are a very promising technology because of the high energy efficiency that can be obtained, together with robustness and reduced emissions. Indeed, when hydrogen is the only fuel, the only release is clean water vapour. Apart from the well known oxide ion conductor electrolyte, high temperature fuel cells can also operate with a protonic conductor electrolyte. These fuel cells, called protonic ceramic fuel cells (PCFC), are especially attractive for operation at intermediate temperatures of 600 °C and below. Many rare-earth doped perovskite materials have been studied as electrolyte for PCFCs because of their high protonic conductivity at about 600 °C and their stability in reducing atmosphere [1]. Doped barium cerates are known for their high protonic conductivity, but are not chemically stable: they react with carbon dioxide to form carbonates. Doped barium zirconates are chemically and mechanically stable, but the protonic conductivity is quite low [2–5]. Solid solutions of barium cerate and barium zirconate exhibit an adequate protonic conductivity as well as sufficient chemical and thermal stability over a wide range of conditions relevant to fuel-cell operation [6–8]. The present study deals with $BaCe_{(0.9-x)}Zr_xY_{0.1}O_{(3-\delta)}$ compounds ($x = 0$ (powder referred to BCZY90), $x = 0.3$ (BCZY63), $x = 0.7$ (BCZY27) and $x = 0.9$ (BCZY09)). A trivalent dopant, yttrium, is used to create oxygen vacancies ($V_O^{\bullet\bullet}$) by charge compensation [9,10].

High temperature proton conducting (HTPC) oxides, such as BCZY, take protons from water vapour or hydrogen. In a wet atmosphere, protons are incorporated by the absorption and dissociation of water molecules. This process, given in Eq. (1), involves the annihilation of oxygen vacancies [11–14].

$$H_2O_{(g)} + V_O^{\bullet\bullet} + O_O{}^{*} \leftrightarrow 2OH_O^{\bullet} \quad (1)$$

Cerates and zirconates are pure proton-conductors only at low temperature [15]. The hydration enthalpy of Eq. (1) is negative; therefore, the equilibrium is shifted to the left when the temperature increases [16–18]. These compounds exhibit p-type conductivity at high oxygen partial pressures (Eq. (2)) and ionic conductivity at intermediate oxygen partial pressures.

$$\frac{1}{2}O_{2(g)} + V_O^{\bullet\bullet} \leftrightarrow 2h^{\bullet} + O_O{}^{*} \quad (2)$$

Thus, the conductivity is given by the following Eq. (3) [1,3,19,20]:

$$\sigma_{total} = \sigma_i + \sigma_p^o \cdot P(O_2)^{1/4} \quad (3)$$

* Corresponding author at: Fuel Cells and Solid State Chemistry Division, Risø National Laboratory for Sustainable Energy, Technical University of Denmark, P.O. 49, DK-4000 Roskilde, Denmark. Tel.: +45 46 77 56 41; fax: +45 46 77 58 58.
E-mail address: sandrine.ricote@risoe.dk (S. Ricote).

0378-7753/$ – see front matter © 2008 Elsevier B.V. All rights reserved.
doi:10.1016/j.jpowsour.2008.11.080

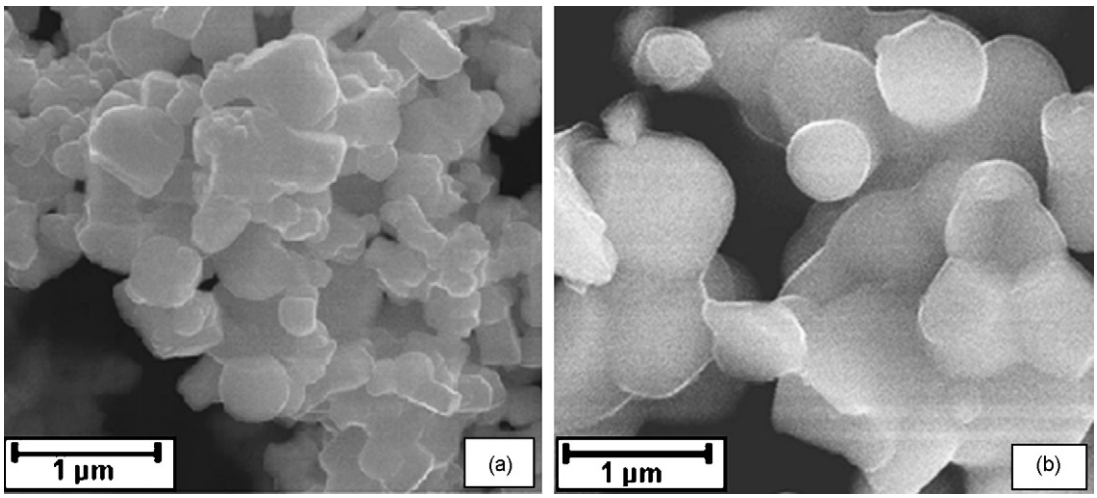

Fig. 1. SEM micrographs of BCZY09 powder (a) and BCZY90 powder (b), 15 keV.

where σ_p^0 is the p-type conductivity at an oxygen partial pressure of 1 atm and σ_i the ionic conductivity, which is the sum of the anionic and the protonic components.

Isotope exchange can be used to determine the protonic contribution of the conductivity. For the case of hydrogen/deuterium (H/D) exchange, the conductivity isotope effect is given by Eq. (4), the apparent isotope effect by Eq. (5) and the proton transport number by Eq. (6) [1,21].

$$\beta = \frac{\sigma_{pr}}{\sigma_{de}} \tag{4}$$

in which the subscripts 'pr' and 'de' refer to protons and deuterons.

$$\alpha = \frac{\sigma_{pr} + (\sigma_{ox} + \sigma_p)}{\sigma_{de} + (\sigma_{ox} + \sigma_p)} = \frac{\sigma_{pr} + (\sigma_{ox} + \sigma_p)}{(\sigma_{pr}/\beta) + (\sigma_{ox} + \sigma_p)} \tag{5}$$

in which the subscripts 'p' refers to the p-type conduction and 'ox' to oxygen conduction.

$$t_{H^+} = \frac{\beta(1-\alpha)}{\alpha(1-\beta)} \tag{6}$$

In this paper, the authors focus on three points:

(1) The morphological and structural characterisation of the $BaCe_{(0.9-x)}Zr_xY_{0.1}O_{(3-\delta)}$ compounds at room temperature. The distortion for $0.2 < x < 0.8$ has been found to be rhombohedral.
(2) The phase transition study in the temperature range 25–600 °C to know the BCZY symmetry in the operating temperature range of PCFCs.
(3) The DC measurements on sintered pellets to determine the different components of the conductivity at the expected operating temperature. The proton transport number has been estimated using the ionic conductivity.

2. Experimental

$BaCe_{(0.9-x)}Zr_xY_{0.1}O_{(3-\delta)}$ powders ($x = 0$, 0.3, 0.7 and 0.9) were synthesized by solid-state reaction. $BaCO_3$ (Aldrich, 99+%), CeO_2 (Aldrich, 99.9%, <5 μm), Y_2O_3 (Sigma–Aldrich, 99.99%), YSZ (Aldrich, submicron powder; 99.5%, 5.3 wt% of yttria) were mixed in stoichiometric proportions for 20 h in a ball mill. The resulting powders were calcined in air at 1400 °C for 24 h, and finally ground. A binder was added to the powders to facilitate the forming. Cylindrical pellets of diameter 13 mm were prepared using a hydraulic press (uniaxial, 350 MPa) and sintered in air at 1700 °C for 6 h.

Scanning electron microscope (SEM, Jeol JSM 6400F) experiments were performed to assess the morphology of the particles and the sintered products. Deposition of carbon was necessary because of the insulating properties of the samples.

Crystallographic phases, lattice parameters and theoretical density were determined using *Celref* software on X-ray diffraction patterns recorded with an X-ray diffractometer Bruker D500 using Cu Kα1 radiation. To complete the structural investigations, the powders were also analysed by Raman spectroscopy, from room temperature to 600 °C. The apparatus was a Jobin-Yvon T64000 working in back-scattering configuration. The 514.5 nm line of an Ar–Kr laser was used as excitation source. The Raman spectra were obtained at a constant excitation power, about 1.2 mW on the sample. A special cell (LINKAM, THMS600) was used for in situ Raman experiments from room temperature up to 600 °C.

The DC conductivity was measured on bar-shaped samples in a 4-point probe arrangement, and was not corrected for the porosity of the samples. Pt paste was applied to each end of the bar, and contacted with Pt leads. Two Pt potential probes at a fixed distance were set on one side of the bar. Different oxygen pressures were obtained by mixing O_2 and N_2 (oxidizing atmosphere) or H_2 and N_2 (reducing atmosphere). The gas mixture was moisturized by bubbling through water held at 13 °C, giving a water vapour partial pressure of ca. 0.015 atm.

The isotope effect on the conductivity was measured by exchanging in D_2/D_2O in place of H_2/H_2O. Holes are created by the ionisation of oxygen according to Eq. (2). Thus, their concentration depends on the concentration of oxygen vacancies which are not filled by the hydration process. This situation leads to almost identical p-type conductivity in the two exchanged states (H_2O and D_2O). *Sigmaplot* software is used for fitting Eq. (3) in the two exchanged states and constraining the same σ_p^0 for both of them.

3. Results and discussion

SEM micrographs of the BCZY powders are presented in Fig. 1(a) and (b): the grain size is about 300 nm for BCZY09, BCZY27 and BCZY63 and about 700 nm for BCZY90. Increasing the cerium content leads to a higher density of the sintered pellets (from 90% for BCZY09 to 95% for BCZY90) as well as a higher particle size (below 1 μm for BCZY09 and several microns for BCZY90).

The room temperature XRD patterns for the BCZY powders are displayed in Fig. 2. No peaks related to the precursors were observed for a 24 h-dwell synthesis. It is worth remembering that barium zirconates crystallise in a cubic structure and barium cerates in an orthorhombic one [19]. The patterns can be indexed with a pseudocubic structure (*Pm3m*) for the BCZY09, BCZY27 and BCZY63

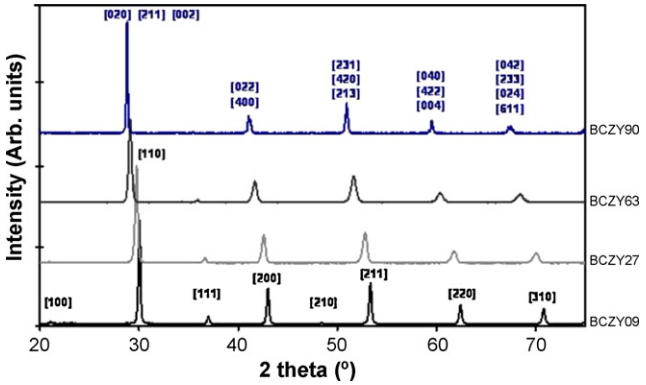

Fig. 2. Room temperature X-ray diffraction patterns for BCZY09, BCZY27, BCZY63 and BCZY90 powders, calcined 24 h at 1400 °C. The diffractograms were vertically shifted for clarity.

compounds, and with an orthorhombic structure (*Pnma*) for the BCZY90 powder. The lattice parameters are summarized in Table 1 and compared to some from the literature. There is good agreement between the cubic lattice parameter for BCZY09 ($a = 0.420$ nm) and those reported by Talib et al. (0.4195 nm) [22] and Schober and Bohn (0.4204 nm) [17], as well as between the orthorhombic lattice parameters ($a = 0.856$ nm, $b = 0.623$ nm and $c = 0.619$ nm) and those from Katahira et al. [7] ($a = 0.8776$ nm, $b = 0.6221$ nm and $c = 0.6224$ nm).

Raman spectra at room temperature (Fig. 3) show great differences as a function of the cerium content as it was shown by Charrier-Cougoulic et al. for $BaCe_{(1-x)}Zr_xO_3$ (BCZ) powders [23]. For these latter ones, the structure at room temperature changes from cubic (*Pm3m*) to rhombohedral (*R-3C*), and finally to orthorhombic (*Imma* and *Pnma*) by increasing the cerium content. No vibrational modes are first-order Raman active for these compounds in the cubic structure, but lowering the symmetry leads to an increasing number of Raman active modes [23,24]. For BCZ powders, Ba–O stretching and O–Ba–O bending modes are mainly found in the 80–150 cm^{-1} range, while O–Ce–O bending, Ce–O stretching and Zr–O stretching modes are in the 350–500 cm^{-1} range [24]. In this study, the spectrum of BCZY09 powder displays only very low intensity and broad Raman bands which is in agreement with a cubic phase. The spectra of BCZY27 and BCZY63 samples display intense Raman bands, revealing a lower symmetry phase. The single band at about 102 cm^{-1} makes one able to assign the spectrum to the rhombohedral phase [23]. These distortions from the cubic structure are too small to be observed on the XRD patterns. Finally, three Raman bands are observed in the 80–150 cm^{-1} range on the BCZY90 spectrum, corresponding to the space group *Pnma* (orthorhombic symmetry) [23].

Phase transitions were studied by Raman spectroscopy from room temperature up to 600 °C. No phase changes were noticeable in this temperature range for the BCZY09 and the BCZY63 compositions. In both cases, the increase of the temperature induced only a continuous shift and broadening of the Raman bands. Fig. 4 presents the spectra for the BCZY27 powder: the single band at about 102 cm^{-1} disappears above 200 °C, resulting in a symmetry change from rhombohedral to cubic. This change to the cubic symmetry leads to the disappearance of all first order Raman bands, as explained before, namely the bands involving the Ce–O and Zr–O vibrational modes at about 365 cm^{-1}. For the BCZY90 powder

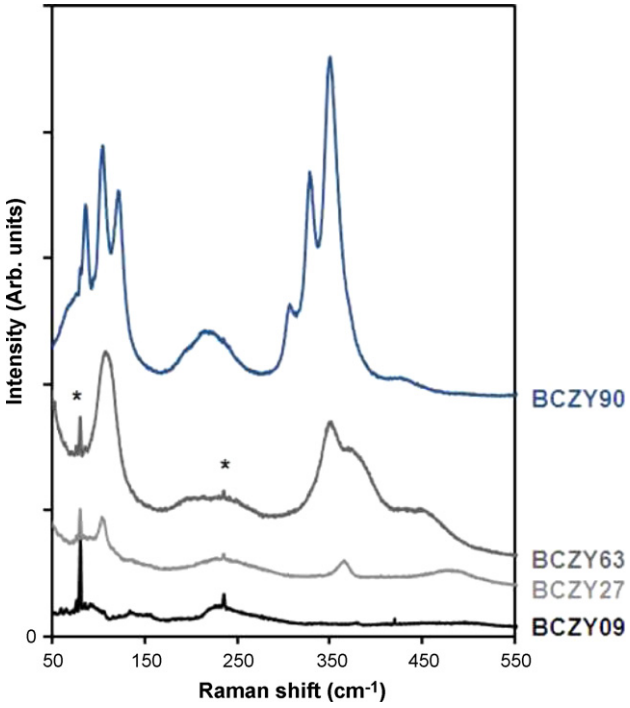

Fig. 3. Room temperature Raman spectra for BCZY09, BCZY27, BCZY63 and BCZY90 powders, calcined 24 h at 1400 °C. The spectra were vertically shifted for clarity. * are indexed as plasma lines.

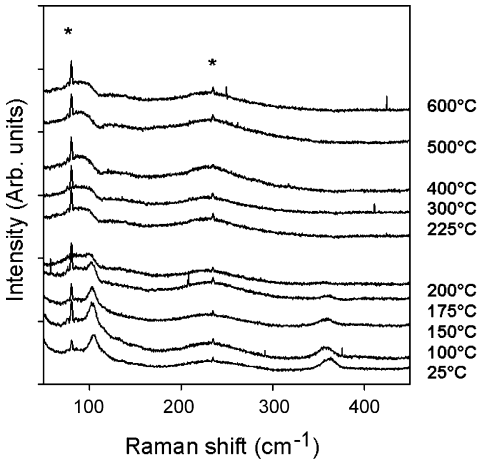

Fig. 4. Raman spectra for BCZY27 composition, from 25 to 600 °C. The spectra were vertically shifted for clarity. * are indexed as plasma lines.

Table 1
$BaCe_{(0.9-x)}Zr_xY_{0.1}O_{(3-\delta)}$ powders lattice parameters and density, determined with XRD for this work.

Powder	x	Lattice parameters (nm)			Density ($g\,cm^{-3}$)	Symmetry	Reference
BCZY09	0.9	0.420			6.15	Pseudocubic	[This work]
BCZY09	0.9	0.4195			6.17	Pseudocubic	[24]
BCZY09	0.9	0.4204			6.13	Pseudocubic	[17]
BCZY27	0.7	0.424			6.21	Pseudocubic	[This work]
BCZY63	0.3	0.433			6.23	Pseudocubic	[This work]
BCZY90	0	0.856	0.623	0.619	6.30	Orthorhombic	[This work]
BCZY90	0	0.8776	0.6221	0.6224	6.12	Orthorhombic	[7]

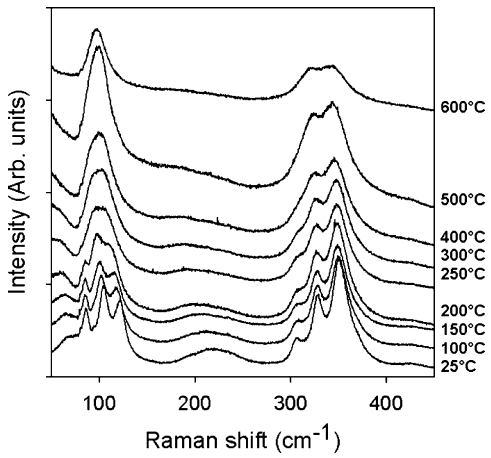

Fig. 5. Raman spectra for BCZY90 composition, from 25 to 600 °C. The spectra were vertically shifted for clarity.

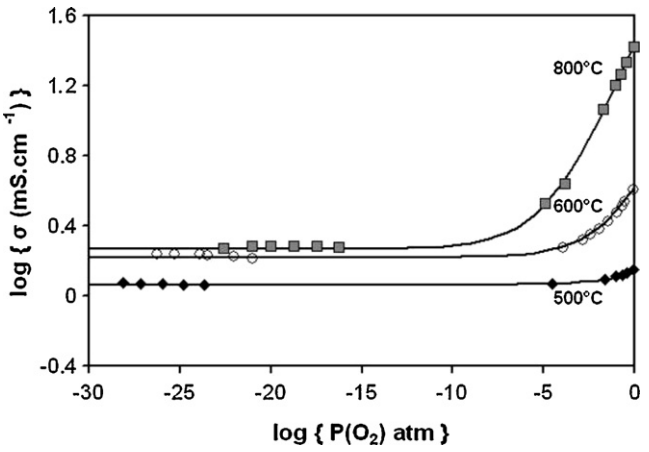

Fig. 6. DC conductivity as a function of the oxygen partial pressure at 500, 600 and 800 °C for the pellet BCZY09 in the H_2O exchanged state. Solid lines correspond to the fits performed using $\sigma_{total} = \sigma_i + \sigma_p^o \cdot P(O_2)^{1/4}$.

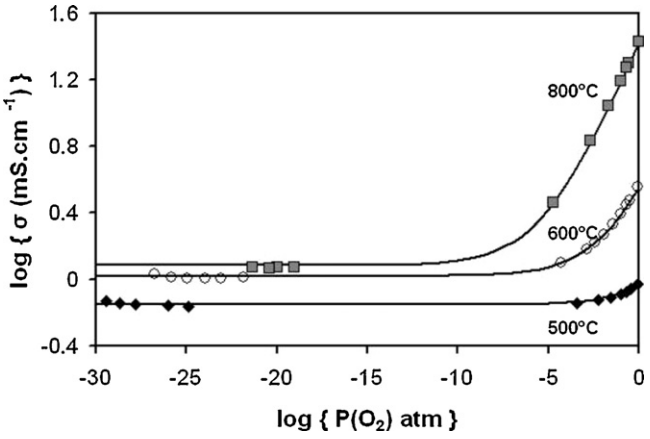

Fig. 7. DC conductivity as a function of the oxygen partial pressure at 500, 600 and 800 °C for the pellet BCZY09 in the D_2O exchanged state. Solid lines correspond to the fits performed using $\sigma_{total} = \sigma_i + \sigma_p^o \cdot P(O_2)^{1/4}$.

(Fig. 5) which displays an orthorhombic structure at room temperature, the disappearance above 200 °C of the three bands in the 80–150 cm^{-1} region reveals the transition towards a higher symmetry phase. Above 300 °C, the narrowing of the band at 100 cm^{-1} together with the disappearance of the small band at 305 cm^{-1} shows a new phase transition. These results are in agreement with the sequence of phase transitions reported by Knight [25] for undoped barium cerates: from *Pnma* to *Imma* at 290 °C, from *Imma* to *R-3C* at 400 °C and finally from *R-3C* to *Pm3m* at 900 °C. Yttrium doping seems to reduce slightly the temperature of phase transitions.

DC conductivity measurements, in H_2O and D_2O exchanged states, were performed at 500 and 600 °C for all the compositions, and also at 800 °C for BCZY09. The DC curves in H_2O exchanged state at 500, 600 and 800 °C are presented for the BCZY09 sample in Fig. 6 and those in D_2O exchanged state in Fig. 7. Table 2 shows the results of the fits for the three temperatures using Eq. (3), as well as the proton transport number range at 600 °C. This last one was estimated using Eq. (6), and setting β between 1.4 and 1.8. Assuming the conductivity is following the Arrhenius law, β is given by Eq. (7):

$$\beta = \frac{A_H}{A_D} \exp^{((Ea_D - Ea_H)/(RT))} \quad (7)$$

With A_X the preexponential factor in X_2O exchanged state, E_X the activation energy in X_2O exchanged state, T the temperature, R the gas constant.

Studies on the isotope effect show the difference $Ea_D - Ea_H$ is assumed to be 4–5 kJ mol^{-1} because of the zero point energy of the H^+ and D^+ species [26], and the ratio A_H/A_D is between 1 and $1/\sqrt{2}$ [13]. Thus, at 600 °C, the average β value is between 1.4 and 1.8.

The proton transport number decreases with the cerium content, meaning an increase of the anionic component of the ionic conductivity. This can be explained by the increase of the lattice free volume with the cerium content. This parameter is obtained by subtracting the ionic volumes of cations and anions in the ionic cell from the overall unit cell volume. It is found to be 34.98 $Å^3$ for barium cerates and 29.25 $Å^3$ for barium zirconates. Sammels et al. [27] showed easier oxygen diffusion in oxides with a larger lattice free volume.

Hole conductivity increases with temperature: hole diffusion is a thermally activated phenomenon. The activation energy, determined plotting ln $\sigma_p^o \cdot T$ versus 1000/T with *Sigmaplot* software, is

Table 2
Ionic conductivity (σ_i (mS cm^{-1})) and hole conductivity (σ_p^o (mS cm^{-1})) values for BCZY pellets at 500, 600 and 800 °C and proton transport number (t_{H+}) values at 600 °C: fits of the DC curves in both exchanged states (H_2O and D_2O) using Eqs. (3) and (6).

Temperature (°C)	Sample	σ_p^o (mS cm^{-1})	$(\sigma_i)_{H_2O}$ (mS cm^{-1})	$(\sigma_i)_{D_2O}$ (mS cm^{-1})	t_{H+} for $\beta = 1.4$	t_{H+} for $\beta = 1.8$
500	BCZY09	0.23	1.18	0.70		
	BCZY27	0.32	1.46	0.91		
	BCZY63	0.15	1.47	1.03		
	BCZY90	0.65	7.42	5.22		
600	BCZY09	2.48	1.66	1.18	1.00	0.65
	BCZY27	2.32	1.89	1.35	1.00	0.64
	BCZY63	1.22	2.33	1.68	0.98	0.63
	BCZY90	4.01	11.71	8.53	0.95	0.61
800	BCZY09	25.30	1.85	1.32		

about 1.14 ± 0.05 eV. This value is similar to the one published by Schober and Bohn [17] for the same compound (1.13 eV). Slightly different values were published by Kurita et al. [28] for calcium zirconate (1.21 eV), and by Wang and Virkar [29] for barium zirconate (1.01 eV).

Oxygen conductivity also increases with temperature, as shown by the increase of the ionic conductivity and the decrease of the ratio $\sigma_{i(H_2O)}$ over $\sigma_{i(D_2O)}$. For HTPC, protons are the main charge carrier only at low temperature. When the temperature is higher than 800 °C, oxygen vacancies are the predominant defects [15].

4. Conclusions

$BaCe_{(0.9-x)}Zr_xY_{0.1}O_{(3-\delta)}$ $(0 \leq x \leq 0.9)$ compounds (referred as BCZY) were synthesized by a solid-state reaction, with a 24 h-dwell at 1400 °C and sintered at 1700 °C. The room temperature XRD patterns obtained for BCZY09, BCZY27 ($x = 0.7$) and BCZY63 ($x = 0.3$) powders showed a cubic or pseudo-cubic structure. However, the corresponding Raman spectra revealed a reduction of the symmetry in BCZY27 and BCZY63 powders due to the increasing cerium content leading to a rhombohedral structure. XRD and Raman results showed the orthorhombic structure (space group *Pnma*) of the zirconium free sample, BCZY90.

In situ Raman experiments from room temperature up to 600 °C, the expected operating temperature range for protonic ceramic fuel cells, revealed no phase transitions for BCZY09 (cubic) and BCZY63 (rhombohedral). By contrast, the symmetry changes from rhombohedral to cubic in the BCZY27 powder. Two-phase transitions were observed for the BCZY90 powder.

The isotope effect underlines a significant protonic conductivity for the BCZY pellets at 500 and 600 °C. The proton transport number range could have been estimated, setting β between 1.4 and 1.8. It increases when temperature and cerium content decrease.

The hole diffusion activation energy was determined (1.14 eV) with the DC measurements at three different temperature.

Acknowledgments

This work was supported by Risø National Laboratory for Sustainable Energy, Technical University of Denmark. It was also funded by the Conseil Régional de Bourgogne and the CNRS.

References

[1] N. Bonanos, Solid State Ionics 145 (2001) 265–274.
[2] K.D. Kreuer, Solid State Ionics 125 (1999) 285–302.
[3] N. Bonanos, K.S. Knight, B. Ellis, Solid State Ionics 79 (1995) 161–170.
[4] M.J. Scholten, J. Schoonman, J.C. van Miltenburg, Thermochim. Acta 268 (1995) 161–168.
[5] T. Shimada, C. Wen, N. Taniguchi, J. Otomo, H. Takahaschi, J. Power Sources 131 (2004) 289–292.
[6] K.H. Ryu, S.M. Haile, Solid State Ionics 125 (1999) 355–367.
[7] K. Katahira, Y. Kohchi, T. Shimura, H. Iwahara, Solid State Ionics 138 (2000) 91–98.
[8] C. Zuo, S. Zha, M. Liu, M. Hatano, M. Uchiyama, Adv. Mater. 18 (2006) 3318–3320.
[9] T. Schober, F. Krug, W. Schilling, Solid State Ionics 97 (1997) 369–373.
[10] I. Kosacki, H.L. Tuller, Solid State Ionics 80 (1995) 223–229.
[11] H. Iwahara, Solid State Ionics 86–88 (1996) 9–15.
[12] P. Colomban, Ann. Chim. Sci. Mat. 24 (1999) 1–18.
[13] A.S. Nowick, Y. Du, Solid State Ionics 77 (1995) 137–146.
[14] K.J. De Vries, Solid State Ionics 100 (1997) 193–200.
[15] H. Iwahara, Solid State Ionics 77 (1995) 289–298.
[16] W.A. Meulenberg, J.M. Serra, T. Schober, Solid State Ionics 177 (2006) 2851–2856.
[17] T. Schober, H.G. Bohn, Solid State Ionics 127 (2000) 351–360.
[18] T. Norby, M. Wideroe, R. Glöckner, Y. Larring, Dalton Trans. (2004) 3012–3318.
[19] D. Lybye, N. Bonanos, Solid State Ionics 125 (1999) 339–344.
[20] N. Bonanos, F.W. Poulsen, J. Mater. Chem. 9 (1999) 431–434.
[21] N. Bonanos, Solid State Ionics 53–56 (1992) 967–974.
[22] I.A. Talib, M. Laidoudi, R. Omar, Solid State Ionics, Mater. Devices (2000).
[23] I. Charrier-Cougoulic, T. Pagnier, G. Lucazeau, J. Solid State Chem. 142 (1999) 220–227.
[24] T. Scherban, R. Villeneuve, L. Abellon, G. Lucazeau, Solid State Ionics 61 (1993) 93–98.
[25] K.S. Knight, Solid State Ionics 74 (1994) 109–117.
[26] A.S. Nowick, A.V. Vaysleyb, Solid State Ionics 97 (1997) 17–26.
[27] A.F. Sammels, R.L. Cook, J.H. White, J.J. Osborne, R.C. Macduff, Solid State Ionics 52 (1992) 111–123.
[28] N. Kurita, N. Fukatso, K. Ito, T. Ohashi, J. Electrochem. Soc. 142 (1995) 1552–1559.
[29] W. Wang, A.V. Virkar, J. Power Sources 142 (2005) 1–9.